JOURNAL OF GUIDANCE, CONTROL, AND DYNAMICS
Vol. 25, No. 1, January–February 2002

Satellite Orbit Determination Using a Single-Channel Global Positioning System Receiver

Mark L. Psiaki*
Cornell University, Ithaca, New York 14853-7501

A proposed satellite orbit determination system has been analyzed, one that uses measurements from a single-channel global positioning system (GPS) receiver. The purpose of this study is to predict the likely efficacy of a low-power autonomous orbit determination system. The system processes the pseudorange outputs of the receiver using an extended Kalman filter. The receiver cycles through different GPS satellites, tracking a new one every 75 s, to achieve observability and reasonable accuracy. The Kalman filter uses a dynamic model of the spacecraft orbit and of the receiver clock's drift. Simulation results predict that the system can achieve peak per-axis position errors that range from 78 to 144 m when in low Earth orbit. The accuracy depends on the level of uncertainty in the orbital dynamics model. The system can also operate in a geosynchronous orbit, but its peak per-axis error degrades to 7 km if the filter neglects solar and lunar gravity terms, and the geosynchronous receiver must use an ovenized crystal oscillator as its clock.

I. Introduction

THE global positioning system (GPS) offers an attractive alternative to ground-based tracking systems for use in many Earth satellite orbit determination applications. Many missions require an accuracy on the order of 100–200 m. The current civilian version of GPS can determine instantaneous position with an accuracy on the order of 10 m when operating in stand-alone mode. This performance is available for virtually all users up to an altitude of 3200 km. These facts give rise to the possibility of performing autonomous GPS-based satellite navigation for many Earth orbiting missions. Such a system could yield significant cost savings through the elimination of ground-based tracking.

An impediment to the use of GPS on Earth-orbiting nanosatellites is the electrical power that is required to run the receiver hardware. Instantaneous point positioning requires a receiver with at least four channels,[1] and most modern terrestrial receivers have 10 or more channels. Such receivers incorporate a general-purpose microprocessor. The average solar power available to a $10\times10\times10$ cm cubic nanosatellite is about 1.5 W (Ref. 2). If one were to implement a typical 10-channel GPS receiver using a currently available space-qualified microprocessor, then the processor power requirements would be on the order of 1 W. Unless the nanosatellite's primary mission were to fly a GPS receiver, this level of power consumption would break the satellite's power budget. The problem only gets worse if one imagines making nanosatellites that are even smaller than 10 cm on a side.

This paper's concept exploits the fact that a savings in the rate of computation can be translated into a savings in electrical power. The electrical power required to operate a typical space-qualified processor scales linearly with clock speed, as does the computation rate (private communication from Bert Schmidt of Synova, Inc.). Therefore, electrical power scales linearly with computation rate if one is willing to reduce the computer clock speed. Most space-qualified microprocessors are fully static devices, which allow arbitrary reductions in their clock speeds.

The goal of the present study is to analyze a GPS orbit determination system that requires much less computing power than a typical multichannel receiver, as much as 90% less. This translates into a 90% savings in electrical power consumption. The method of reducing the computation load is to scale the system back to just one receiver channel. To achieve observability and allow the determination of spacecraft position and velocity, the system will have to switch its one channel to track different GPS satellites over the course of time. Normally such an approach would present serious problems to a dynamic user vehicle. In the case of orbit determination, however, there is hope that such a system could be made to work because there exist accurate models of orbital dynamics.

An added benefit of the proposed system is that it could enable near-term use of a real-time software GPS receiver for autonomous orbit determination. The first real-time software receiver has been successfully tested only recently.[3] Software receivers offer benefits such as design flexibility, reconfigurability, and a reduction in the number of special-purpose chips that are needed in the receiver. They also require much more computing power in the system's general-purpose microprocessor. Currently available space-qualified microprocessors would be hard pressed to perform all of the functions of a multichannel software receiver, but some of them would be capable of implementing a single-channel software receiver because the computing requirements scale linearly with the number of channels.

This study considers a Kalman-filter-based system and evaluates its performance using a truth-model simulation. The Kalman filter estimates the satellite orbit from a time series of tracking data from the single receiver channel. The investigation considers the following aspects of performance: the accuracy in typical low Earth orbits (LEO), the ability to converge from large initial errors, the required level of receiver clock stability (which also impacts power), the effects of various changes of system configuration, and the effects of differing orbits, including geosynchronous Earth orbits (GEO). The truth model includes the following error sources in its dynamics and measurement models: higher-order Earth gravity terms, solar and lunar gravity, solar radiation pressure, drag model error, receiver clock drift, ionospheric delay, carrier phase multipath, receiver thermal noise, and small GPS constellation ephemeris and clock errors.

Numerous studies of GPS-based orbit determination have been carried out (see, for example, Refs. 4–8). Some of these studies have used actual flight data.[5,7] Simulation has been used as a way to evaluate proposed system designs.[6–8] A number of these studies have concentrated on high-end systems that achieve very precise orbit determination accuracy (on the order of centimeters) through the use of multichannel flight receivers, carrier phase measurements, and differential corrections from ground-based receivers.[4,5] Systems that employ a single onboard receiver have also been studied.[6–8] References 6 and 8 considered performance when the system does not always simultaneously track the required minimum of four GPS satellites; their consideration of high-altitude cases forced them to consider this situation, as will be discussed later in this paper. The

Received 29 June 2000; revision received 9 April 2001; accepted for publication 12 April 2001.

*Associate Professor, Sibley School of Mechanical and Aerospace Engineering. Associate Fellow AIAA.

study of Ref. 7 envisions a low-power receiver, in the spirit of the present study. Its accuracy is in the 100-m range, but it is not fully autonomous, nor does it operate in real time. Instead, it requires that a very sparse data set be telemetered to the ground for extensive postprocessing to deduce orbit.

The present study makes several new contributions to the field of GPS-based orbit determination. First, it considers the performance of a single-channel system for a range of Earth orbits varying from LEO to GEO. Second, it explores whether the use of carrier phase measurements offers any performance improvements for this stand-alone system. Third, it makes an improvement in the mathematical technique for shuffling the carrier phase ambiguity into and out of the Kalman filter state vector at the beginning and end of the tracking interval of a particular GPS satellite.

The remainder of this paper consists of three main sections plus conclusions. Section II describes the hardware, software, and Kalman filter of the system that is being proposed. Section III presents the truth-model simulation that has been used to evaluate the system. Section IV presents the results of the simulation study. Section V summarizes the paper's developments and results.

II. Orbit Determination System Design

A. Hardware and Software Functions and Interactions

The proposed system consists of several interacting pieces of hardware and software. The basic hardware components and their interactions are shown in Fig. 1. The signal $y_{L1}(t)$ is the GPS L1 signal, and $y_{IF}(t)$ is a down-converted version of this signal that has been bandpass filtered, rescaled, and digitized.

The microprocessor must multitask a number of different software processes. It uses three broad categories of software: the signal acquisition, tracking, and data demodulation software; the software that schedules which satellite to track; and the orbit determination Kalman filter software.

The acquisition, tracking, and demodulation software operates much like that of a normal receiver except for one significant difference: The signal acquisition process is assumed to be aided by the Kalman filter. Aiding gives the acquisition a good estimate of a signal's Doppler shift, which reduces the required time to lock onto a signal. The overall system's success is dependent on its ability to acquire and lock onto a signal quickly. Throughout this study, it has been assumed that signal lock can be achieved in 30 s.

In LEO, there will normally be a number of satellites in view, which is why it is necessary to have a scheduling module that picks which satellite to track at any given time. A simple algorithm has been used to accomplish this task. It uses three principal inputs. One input is the rough ephemeris data for the entire GPS constellation, which are located in an almanac that is resident in the microprocessor's memory. Another input is the Kalman filter's estimate of the satellite position. The third input is the target nominal tracking interval for a single satellite.

The tracking selection algorithm operates as follows. It allows the receiver to track a particular GPS satellite's signal until the target tracking duration has been achieved or until the signal's signal-to-noise ratio (SNR) becomes too low to maintain lock. It then cycles through the list of satellite pseudo-random number (PRN) codes in the order of ascending PRN identifier (ID) numbers. It selects the next available satellite that, according to the constellation almanac and the estimated user spacecraft location, should be in view with sufficiently high SNR to allow tracking ($\geq$37 dB Hz). This SNR calculation takes into account the gain pattern of each GPS satellite's L1 antenna, occultation of the signal by the Earth, the gain pattern of the user antenna, and an estimate of the user spacecraft attitude. The list of PRN ID numbers is repeated cyclically in the scheduler. After the visible GPS satellite with the highest PRN ID number has been tracked, the algorithm starts over again at the bottom of the list. If the only visible satellite is the one that is already being tracked, then the scheduling algorithm will reselect the currently tracked satellite. In this case, the receiver will continue to track the current satellite for longer than the target interval.

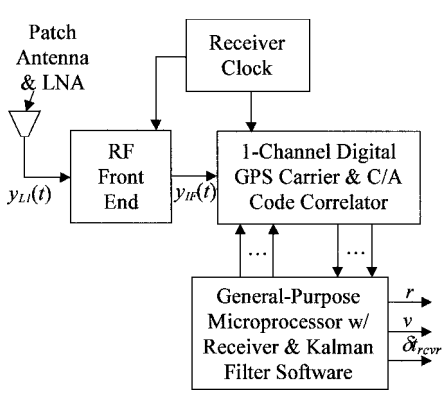

Fig. 1 Block diagram of GPS orbit determination system's hardware.

The Kalman filter estimates the spacecraft's position and velocity and corrections to the receiver clock. It operates on pseudorange data, time data, and possibly carrier phase data. This data is provided by the digital correlator. The filter also needs to know the ephemeris and the clock corrections for the tracked GPS satellite. These data are provided by the demodulation software, which decodes the GPS signal's navigation message. Each signal must be tracked for at least 30 s so that the full navigation message can be decoded.

B. Kalman Filter Design

The Kalman filter that is used in this system is a sampled-data extended Kalman filter that stores its state estimate and state error covariance in the square-root information filter (SRIF) format. The SRIF for linear discrete-time systems is described in Ref. 9, and an extension to handle nonlinear sampled-data systems is described in Ref. 10.

Two modifications of the basic filter algorithm have been used for the problem at hand. One allows it to append the carrier phase ambiguity state for the tracked satellite onto the state vector at the start of a tracking interval and to delete it from the state vector at the end of the interval. The other modification is to include the option to use a nonlinear iteration in the measurement update to aid convergence from large initial errors. Both of these modifications are described later in this section.

1. *State Vector and Dynamic Model*

The filter operates on a state vector, alternatively propagating it between measurement sample times based on a dynamic model and then updating it using the measured data in conjunction with a measurement model. This filter's state vector is

$$\boldsymbol{x} = \begin{bmatrix} \boldsymbol{r} \\ \boldsymbol{v} \\ \delta t_{\text{rcvr}} \\ \delta f_{\text{rcvr}} \\ N^j \end{bmatrix} \tag{1}$$

where $\boldsymbol{x}$ is the 9×1 state vector, $\boldsymbol{r}$ is the 3×1 Cartesian position vector of the user spacecraft in Earth-centered inertial coordinates (ECI), $\boldsymbol{v}$ is the 3×1 Cartesian velocity vector of the user spacecraft in ECI coordinates, δt_{rcvr} is the receiver clock error, δf_{rcvr} is the receiver frequency error expressed as a fraction of its nominal frequency, and N^j is the carrier phase ambiguity for GPS satellite j, which is the currently tracked satellite. The state vector gets shortened to an 8×1 vector by deletion of N^j whenever the receiver is not tracking a GPS signal.

Before developing a dynamic model of the system, one needs to know the relationship between the receiver clock's time and true GPS time, which is universal time plus a few leap seconds. Suppose that t is the true GPS time and that t_{rcvr} is the receiver clock's estimate of t. Then the relationship between these two times and the receiver clock error is

$$t = t_{\text{rcvr}} - \delta t_{\text{rcvr}} \tag{2}$$

The filter uses a nonlinear differential equation to model the system's dynamics. It numerically integrates this equation between sample intervals to develop an equivalent nonlinear discrete-time difference equation of the system. The differential equation model

of this system is expressed using t_{rcvr} as its independent variable. This is necessary because the system keeps track of events using t_{rcvr}. If one uses the prime notation to denote differentiation with respect to t_{rcvr}, then the system's differential equation model is

$$\boldsymbol{r}' = \boldsymbol{v}[1 - (\delta f_{\text{rcvr}} + w_t)] \tag{3a}$$

$$\boldsymbol{v}' = [\boldsymbol{g}(\boldsymbol{r}) + \boldsymbol{a}_{\text{drag}}(\boldsymbol{r}, \boldsymbol{v}; C_D S/m) + \boldsymbol{w}_v][1 - (\delta f_{\text{rcvr}} + w_t)] \tag{3b}$$

$$(\delta t_{\text{rcvr}})' = \delta f_{\text{rcvr}} + w_t \tag{3c}$$

$$(\delta f_{\text{rcvr}})' = w_f \tag{3d}$$

$$(N^j)' = 0 \qquad \text{for} \qquad \text{any } j \tag{3e}$$

The function $\boldsymbol{g}(\boldsymbol{r})$ is the gravitational acceleration, and the function $\boldsymbol{a}_{\text{drag}}(\boldsymbol{r}, \boldsymbol{v}; C_D S/m)$ is the aerodynamic drag acceleration. The parameters C_D, S, and m are, respectively, the drag coefficient, the aerodynamic reference area, and the mass of the user spacecraft. The 3×1 vector $\boldsymbol{w}_v(t)$ is a white-noise process disturbance; it is the unmodeled component of the user spacecraft's acceleration. The first two equations model the user spacecraft's point-mass translational kinematics and its $F = ma$ dynamics. The third and fourth equations model the receiver clock's drift.[11] The scalars $w_t(t)$ and $w_f(t)$ are white-noise process disturbances that drive the drift model. The last equation indicates that the carrier phase ambiguity is constant during a given tracking interval.

The white noise inputs are uncorrelated with each other, and their statistics are given by

$$E\{\boldsymbol{w}_v(t)\} = 0, \qquad E\left\{\boldsymbol{w}_v(t)\boldsymbol{w}_v^T(\tau)\right\} = Q_v\delta(t-\tau) \tag{4a}$$

$$E\{w_t(t)\} = 0, \qquad E\{w_t(t)w_t(\tau)\} = 0.5h_0\delta(t-\tau) \tag{4b}$$

$$E\{w_f(t)\} = 0, \qquad E\{w_f(t)w_f(\tau)\} = 2\pi^2 h_{-2}\delta(t-\tau) \tag{4c}$$

where Q_v is a 3×3 positive definite matrix and h_0 and h_{-2} are positive scalars that Ref. 11 uses to quantify oscillator stability.

The gravity model $\boldsymbol{g}(\boldsymbol{r})$ only includes the $1/\|\boldsymbol{r}\|^2$ central force and the J_2 oblateness effect. This simplification reduces the computational load of the filter, but it also impacts the filter's performance. The philosophy of this design is to minimize the computational load while still maintaining a certain level of estimation accuracy. As will be seen in the results section, this modeling simplification can be tolerated in LEO, but it causes serious problems at higher altitudes, when there are long data gaps during which no GPS satellites are visible. A more accurate gravity model could improve the performance in such cases, but no such model is considered for use in this Kalman filter because the goal is to design a relatively simple estimation system.

The drag model $\boldsymbol{a}_{\text{drag}}(\boldsymbol{r}, \boldsymbol{v}; C_D S/m)$ uses a logarithmic interpolation of the 1976 U.S. Standard Atmosphere[12] to derive density. It computes the drag based on the assumption that the atmosphere is at rest with respect to the Earth. An a priori modeled value is used for the inverse ballistic coefficient, $C_D S/m$.

2. *Measurement Model*

Two types of position measurements are available from a typical GPS receiver. One is pseudorange ρ^j. It is the distance from the user spacecraft to tracked GPS spacecraft j as determined by the time of flight of the radio signal. The time of flight is based both on the receiver clock, which is inaccurate, and on the GPS satellite j clock, which is very accurate. A mathematical model for this measurement is

$$\rho^j = \sqrt{(\boldsymbol{r} - \boldsymbol{r}^j)^T(\boldsymbol{r} - \boldsymbol{r}^j)} + c\delta t_{\text{rcvr}} + n_\rho \tag{5}$$

where $\boldsymbol{r}^j$ is the position of GPS satellite j in ECI coordinates at the time that the signal left the satellite, c is the speed of light in vacuum, and n_ρ is the pseudorange measurement error. The vector $\boldsymbol{r}^j$ can be derived from the decoded navigation message. The measurement error is composed of several constituents: ionospheric delay, GPS satellite ephemeris and clock errors, and receiver-generated noise.[13] Multipath error, although significant in terrestrial pseudorange measurements, is probably not a significant error source for spacecraft. The filter assumes that the pseudorange measurement error is a discrete-time white-noise process with zero mean and a standard deviation of σ_ρ.

The other available measurement is the phase of the carrier signal, ϕ^j. If the phase is measured in cycles, then its mathematical measurement model is

$$\lambda_{L1}\phi^j = \sqrt{(\boldsymbol{r} - \boldsymbol{r}^j)^T(\boldsymbol{r} - \boldsymbol{r}^j)} + c\delta t_{\text{rcvr}} - N^j + n_\phi \tag{6}$$

where $\lambda_{L1} = 19.03$ cm is the carrier wavelength of the L1 signal and n_ϕ is the carrier phase measurement error. The significant components of the carrier phase measurement error are ionospheric phase advance, user-spacecraft-generated multipath reflections, and receiver-generated noise. Similar to the pseudorange error, this error source is assumed to be a discrete-time white-noise process with zero mean and a standard deviation of σ_ϕ. This filter assumes that n_ρ and n_ϕ are uncorrelated. Strictly speaking, this is not true; the ionospheric components of the two measurement errors are negatively correlated with a correlation coefficient of -1.

3. *Comments About the Use of Carrier Phase Measurement*

Note that the consideration of carrier phase measurements in this study is unusual. Carrier phase is normally used only in precise orbit determination systems that often can track four or more GPS satellites simultaneously and that use differential corrections from ground-based receivers.[4,14] The use of carrier phase for stand-alone civilian systems was considered to be pointless when selective availability (SA) was in effect because SA dominated both σ_ρ and σ_ϕ and made them equivalent for long tracking intervals. Now that SA has been turned off, σ_ϕ is likely to be much smaller than σ_ρ (except for the constant average of its ionospheric component, which can be treated as part of N^j). This opens up the possibility that carrier phase may improve the accuracy of a stand-alone civilian system. For example, carrier phase may improve the velocity estimation accuracy.

Two versions of the filter have been developed to evaluate whether carrier phase measurements provide any benefit. One version uses carrier phase, as already described, and the other does not. This second filter provides a benchmark for assessing the benefits of carrier data.

There are a few fine points about how best to fold the carrier phase ambiguity into and out of the state vector at the beginning and end of a tracking interval. Reference 4 appends the ambiguity to the state vector and initializes its variance to an artificially high value. There is a more exact way to do this in the context of an SRIF. The procedure of Ref. 4 is optimal in the limit as the initial variance of the phase ambiguity approaches infinity. Unfortunately, in the context of a Kalman filter that stores the state estimation error covariance matrix or its square root, it is not possible to let the initial phase ambiguity variance actually go to infinity.

An SRIF allows one to exactly achieve an infinite initial variance for the carrier phase ambiguity. The SRIF simply appends N^j to the state vector and appends a column of zeros to its a priori square root state information matrix. This operation exactly achieves an infinite initial variance because an SRIF stores square roots of information matrices instead of covariance matrices, and a covariance of infinity corresponds to an information value of zero. The appended column of zeros poses no problem to the SRIF because, after a measurement update has been performed, the a posteriori square root information matrix becomes nonsingular.

The SRIF design makes it slightly more difficult to delete the ambiguity at the end of a given satellite's tracking interval. A standard covariance representation can simply delete the ambiguity from the state vector while simultaneously deleting the corresponding rows and columns from the state estimation error covariance matrix. The SRIF algorithm must first isolate the phase ambiguity in its state information equation. Suppose that the state information equation takes the form

$$R\boldsymbol{x} = \boldsymbol{z} - \boldsymbol{n} \tag{7}$$

where R is the square root information matrix, $\boldsymbol{z}$ is a vector that stores an equivalent of the current state estimate, and $\boldsymbol{n}$ is a zero-mean, unit-variance, uncorrelated random error vector. Note that

$R^{-1}z$ is the state estimate and that $R^{-1}(R^{-1})^T$ is the state estimation error covariance matrix. Orthogonal factorization must be used to isolate the phase ambiguity in the R matrix. This is accomplished by using a householder orthonormal transformation H to transform R so that the last column of $R_{\text{tr}} = HR$, the column associated with N^j, has zeros in all of its entries below the first row. If the vector z also gets transformed, $z_{\text{tr}} = Hz$, then the correct square root information matrix after the deletion of N^j is R_{tr} with its first row and last column deleted, and the corresponding vector is z_{tr} with its first row deleted.

Note that there are other possible ways to make use of carrier phase data. For example, one could implement carrier smoothing of the pseudorange measurements. The philosophy of this design is to make optimal use of both the carrier phase measurements and the filter's dynamic model. This is the same philosophy as has been adopted in Ref. 4.

4. System Observability

The observability of this system has been checked. The observability analysis calculates the system's observability gramian for a linearization of the dynamics and measurement equations about the estimated state time history. The gramian has been calculated for an observation vector that includes all of the carrier phase ambiguities for all of the GPS satellites that get tracked during the interval of interest. The gramian must be nonsingular for observability to hold.[15]

The system has been found to be observable for representative LEO cases. The gramian starts out being singular because the system initially tracks only one GPS spacecraft, but by the time it has locked on to the fourth spacecraft, the gramian is clearly nonsingular.

5. Iterated Nonlinear Measurement Update

It is sometimes beneficial to use a special form of the SRIF measurement update that employs nonlinear least-squares methods. This procedure amounts to an SRIF implementation of what is commonly known as an iterated extended Kalman filter. Suppose that the a priori state error information equation is $\tilde{R}\boldsymbol{x} = \tilde{\boldsymbol{z}} - \tilde{\boldsymbol{n}}$. Then the solution of the following nonlinear least-squares problem constitutes the nonlinear measurement update, in which $\boldsymbol{x}$ is found to minimize

$$J_{LS} = 0.5(\tilde{R}\boldsymbol{x} - \tilde{z})^T(\tilde{R}\boldsymbol{x} - \tilde{z}) + \left(1/2\sigma_\rho^2\right)\left[\sqrt{(\boldsymbol{r} - \boldsymbol{r}^j)^T(\boldsymbol{r} - \boldsymbol{r}^j)} + c\delta t_{\text{rcvr}} - \rho^j\right]^2 + \left(1/2\sigma_\phi^2\right)\left[\sqrt{(\boldsymbol{r} - \boldsymbol{r}^j)^T(\boldsymbol{r} - \boldsymbol{r}^j)} + c\delta t_{\text{rcvr}} - N^j - \lambda_{L1}\phi^j\right]^2 \quad (8)$$

This nonlinear least-squares problem can be solved using an iterative numerical optimization procedure such as the Gauss–Newton method (see Ref. 16). As a point of reference, the standard, that is, noniterated, measurement update of an extended Kalman filter can be viewed as being a single Gauss–Newton step starting from an initial guess equal to the a priori state estimate. Two Gauss–Newton steps are used in this paper's iterated filter, and the first step starts from the a priori state estimate.

The iterated update uses an adaptive step size algorithm that approximately minimizes the least-squares function along each Gauss–Newton search direction (see Ref. 16). Adaptive step size methods are known to improve convergence robustness in the general field of nonlinear optimization. The same holds true in the case of iterated extended Kalman filtering. The improved ability to converge can be significant when the filter starts with a poor initial state estimate.

6. Filter Tuning

Proper tuning of the filter is necessary to achieve reasonable accuracy. The filter gets tuned by selection of its initial a priori state estimation error square-root information matrix and by selection of its process and measurement noise intensities, Q_v, h_0, h_{-2}, σ_ρ, and σ_ϕ.

The initial state estimation error variances, whose inverse square roots are the diagonal elements of the initial square-root information matrix, have been sized to reflect the statistics of the actual errors between the filter's initial state estimate and the initial state of the truth model. This assumes that the user has a good idea of the accuracy of the initial state estimate.

Similarly, the clock drift intensities h_0 and h_{-2} have been selected to be the same as are used in the truth model. This assumes that the user has tested the receiver clock and characterized its stability by selecting appropriate values of these two parameters.

The intensity of the acceleration process noise Q_v has been sized based on the expected level of the acceleration error in the filter's models and based on the expected average time interval that the receiver needs to have tracked four different GPS satellites. This time interval has been chosen for the heuristic reason that four is the minimum number of GPS signals needed for standard point positioning. This method of tuning effectively tells the filter to wait until it sees four GPS satellites before it decides to attribute a measurement anomaly to the effects of unmodeled accelerations.

These considerations lead to the following method of picking Q_v. Suppose that the average interval for tracking a total of four GPS satellites is Δt_4 and that the expected level of acceleration uncertainty in the filter model is a_{err}. Then the matrix Q_v is set equal to the identity matrix times the constant $0.25(a_{\text{err}})^2\Delta t_4$. In LEO, the acceleration errors are dominated by uncertainty in the Earth gravity model, and the value $a_{\text{err}} = 10^{-4}$ m/s^2 is a reasonable measure of this uncertainty. If $\Delta t_4 = 300$ s, then $Q_v = 7.5 \times 10^{-7} \times I$ m^2/s^3. In practice, values within a factor of three of this value have all yielded fairly similar performance for LEO cases. This tuning value is reasonable for any orbit in the altitude range from 350 up to 3200 km.

For altitudes above 3200 km, the tuning becomes more difficult because Δt_4 can become very large due to gaps in the coverage of the GPS constellation. There do not seem to be any good rules of thumb for such cases. Values on the order of $Q_v = 3 \times 10^{-8} \times I$ m^2/s^3 have given the best results in GEO, and values on the order of $10^{-7} \times I$ m^2/s^3 have worked reasonably well in highly elliptical orbits that spend some time below 3200-km altitude and much more time above that altitude.

The last two tuning parameters are the measurement noise intensities σ_ρ and σ_ϕ. These quantities are tuned partly based on a priori measurement error estimates and partly based on the receiver's measured SNR and known tracking loop bandwidths. The receiver can monitor the SNR of the 1000-Hz accumulations that its digital correlator chip produces, and it can use this SNR to predict the noise contributions to the pseudorange and carrier phase measurement errors. These noise contributions are then root sum squared with a priori measurement error standard deviations to produce σ_ρ and σ_ϕ.

In the case of σ_ρ, the largest contributor to its a priori component is the anticipated ionospheric error. Estimates for this error range from an rms value of about 3 or 4 m at a 350-km altitude down to less than 1 m at a 1000-km altitude. In GEO, the rms ionospheric error is likely to be large, perhaps as much as 10 m, because a given GPS satellite is visible to the user satellite only when the line-of-sight vector between them passes near the Earth and, therefore, through a significant portion of the ionosphere. For an elliptical orbit, the expected ionospheric error component at its lowest altitude is used to tune σ_ρ. Note that the numbers quoted here come from an approximate ionospheric model that will be described later in this paper. These values assume that the receiver does not compensate for ionospheric effects.

The a priori component of σ_ϕ has been sized based on the expected levels of carrier phase multipath error from reflections off of the user spacecraft. These have been sized conservatively at 0.010 m based on information given in Ref. 17.

III. Truth-Model Simulation for Use in Filter Evaluation

A. Philosophy of Truth-Model Filter Evaluation

The truth model generates data for use in evaluating the filter. It simulates GPS tracking data, the truth position and velocity states of the user spacecraft, and the truth states of the GPS receiver's clock error. Its dynamics and measurement models incorporate effects that are not included in the filter. The filter processes the simulated tracking data and produces estimates of the position, velocity, and clock error states. The filter performance can be measured by comparison

of these estimates to their truth-model counterparts. In addition, the filter's tuning can be evaluated for rough consistency by comparing the statistics of the actual errors to the predicted error variances that the filter computes in its normal course of operation.

B. Dynamics Truth Model

The truth dynamic model is like that given in Eqs. (3a–3e), but with four differences: First, the gravity model includes a 30×30 spherical harmonic expansion of the Earth's gravity field and solar and lunar point-mass effects. The coefficients of the Earth gravity model are those of NASA's EGM 96 model.[18] Second, an acceleration due to solar radiation pressure is included. It produces accelerations on the order of 10^{-7} m/s^2 during orbit day. Third, the truth drag model uses different values of $(C_D S)/m$ than are used by the filter. The filter's $(C_D S)/m$ values have errors that range from -40 to $+67\%$ of the truth-model values. Fourth, the random white-noise acceleration error in Eq. (3b), $\boldsymbol{w}_v$, is eliminated.

The dominant discrepancy between the truth orbital dynamics model and the filter's orbital dynamics model is the difference in their gravity fields. This is true at all altitudes down to the lowest altitude of interest, 350 km. In LEO orbits, the resulting acceleration differences are on the order of 10^{-4} m/s^2 and are due to nonspherical Earth effects. In GEO orbits, the differences are mainly due to solar and lunar gravity effects and are on the order of 10^{-5} m/s^2.

The simulation uses a discrete-time random sequence from a random number generator to simulate the effects of the process noise terms that drive the receiver clock drift, w_t and w_f. Two different clock stability truth models have been used in this study. One has drift parameters representative of a temperature-compensated crystal oscillator (TCXO): $h_0 = 2 \times 10^{-19}$ s and $h_{-2} = 2 \times 10^{-20}$ /s (Ref. 11). Throughout the remainder of this paper, this clock model is referred to as the TCXO. The drift parameters of the other model roughly correspond to those of an ovenized crystal oscillator (OXO) that is currently in use in a space-based GPS receiver: $h_0 = 2 \times 10^{-22}$ s and $h_{-2} = 6.1 \times 10^{-22}$/s. This more stable receiver clock model is referred to as the OXO throughout the remainder of this paper.

C. Measurement Truth Model

The simulation's measurement model is based on Eqs. (5) and (6). It uses the dynamic model's truth values for $\boldsymbol{r}$ and δt_{rcvr} in these equations. The value of N^j is chosen arbitrarily so that the measured $\phi^j = 0$ at the start of a tracking interval. The complicated parts of the measurement truth model lie in its calculation of the GPS satellite position $\boldsymbol{r}^j$, the pseudorange error n_ρ, and the carrier phase measurement error n_ϕ.

The truth-model simulation actually computes two values of the GPS satellite position. One is the truth value that it uses in the measurement equations, and the other is a reported value that it sends to the receiver via its navigation message. The truth value of $\boldsymbol{r}^j$ is obtained using the Yuma almanac for week nine.[19] The reported value is produced using ephemerides that are slightly perturbed from the truth ephemerides. These perturbations produce rms position errors for the GPS satellites on the order of 3 m over a 12-h period, which is consistent with experimentally obtained results.[20]

The simulated measurement errors are sums of several components. One is a random component that is based on the SNR of the received signal and on the receiver's tracking loop bandwidth. The bandwidths of the carrier and code tracking loops have both been fixed at 1 Hz. The received SNR is computed by taking actual experimental data from a typical roof top patch antenna and scaling it based on the differing distance from the user satellite to the GPS satellite and based on the location of the user satellite in the GPS satellite's antenna gain pattern. The user satellite's antenna gain pattern also is considered, but only as a go/no-go criterion that checks whether the GPS satellite is within the presumed 65-deg half-width of the gain pattern's conical field of view (FOV). The noise-induced pseudorange measurement errors are no more than 2 m rms in GEO, and they get as low as 0.5 m rms in LEO. The noise component of the carrier phase error is extremely low, ranging from 1×10^{-4} m rms in LEO to 4×10^{-4} m rms in GEO.

Another component of the measurement error truth model is an ionospheric model. This model is a modified version of the ionospheric correction model that is commonly used in single-frequency receivers.[21] It incorporates an altitude dependence of the electron density that has a scale height of 120 km below 1000 km of altitude, and a scale height of 2000 km above this altitude. The ionospheric delay is computed from this model by integrating along the line of sight from the user spacecraft to the tracked GPS satellite. This ionospheric delay is then multiplied by the speed of light. The resultant distance is added to n_ρ to model the code delay and subtracted from n_ϕ to model the carrier phase advance.

Another component of both measurement errors is the residual clock error of the tracked GPS satellite. This has been modeled as a second-order polynomial that varies slowly. The range equivalent error can have a magnitude as large as 4 m, and each satellite's clock error can vary by as much as 1.5 range-equivalent meters in a day.

The final simulated measurement error is the carrier phase multipath error. This error is modeled as being a function of the orientation in user spacecraft coordinates of the line-of-sight vector to the tracked GPS satellite. The attitude of the user satellite is assumed to be nadir pointing. The multipath error function is defined by a random, but constant, spherical harmonic expansion of up to seventh degree. Two different multipath models have been used. They both have maximum carrier phase multipath errors of 0.01 m, which is consistent with results reported in Ref. 17.

IV. Simulation-Based Performance Evaluation of the System

A. Typical LEO Case

The following example is representative of many LEO cases. The spacecraft orbit has an apogee altitude of 656 km, a perigee altitude of 607 km, and an inclination of 58 deg. The receiver clock is the TCXO. The Kalman filter processes one measurement sample every 15 s. The receiver nominally tracks one new GPS satellite every 75 s. The first 45 s of this period are spent acquiring the signal, and the last 30 s are spent tracking it, which yields three actual measurements per satellite. If the SNR becomes too low to maintain lock before the signal has been tracked for 30 s, then the data are discarded under the assumption that the receiver may have failed to decode the full navigation message. The Kalman filter uses the carrier phase data, but does not use the iterated measurement update.

Figure 2 shows the position error time history for this case broken into its three components, along track (the solid curve), cross track (the dash-dotted curve), and altitude (the dotted curve). The initial position error is 15 km, and the initial velocity error is 17 m/s. As shown in Fig. 2, the filter quickly converges from these initial errors to reach an accuracy of better than 200 m in the first tenth of an hour. This is the time that is required to finish tracking four GPS satellite signals and to start on the fifth. This rapid convergence illustrates that the system's observability has mostly to do with how many GPS satellites the receiver tracks in a given time period. The filter takes about one-half of an hour to settle into steady-state operation. The peak steady-state errors for this case are 64-m along track, 128-m across track, and 72 m in altitude. The corresponding rms component errors are 19, 42, and 23 m.

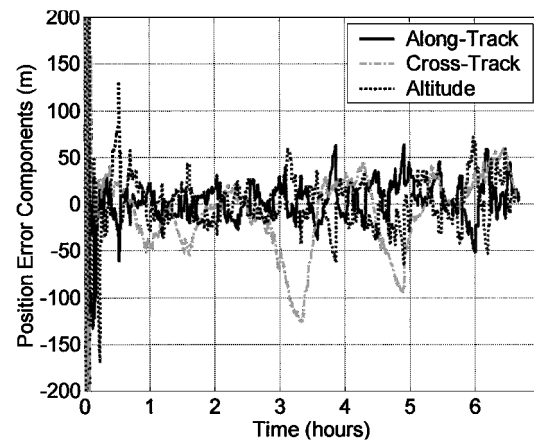

Fig. 2 Position error performance for typical LEO case.

This represents a significant performance degradation in comparison to a multichannel receiver. A benchmark simulation of a 12-channel receiver operating in point-solution mode has been run for all cases that have been considered in this paper. In the case that corresponds to Fig. 2, the point solution achieves peak position errors of 5-m along track, 5-m across track, and 13 m in altitude. The corresponding rms position errors are, respectively, 1.4, 1.7, and 3.5 m. Thus, the proposed system's accuracy is about an order of magnitude worse than that of the standard multichannel point solution. This level of performance differential between the two systems is typical of many LEO cases.

The proposed system would be useful for many missions despite this degraded performance. Many spacecraft require orbit determination accuracy on the order of 100–200 m. This paper's system would serve the needs of such spacecraft at a reduced level of power consumption.

The present system compares favorably with the microGPS receiver of Ref. 7. The position accuracies of the two systems are similar, but the time transfer accuracy of the present system is much better, on the order of 10^{-6} s vs 0.05 s for the microGPS system.

The position errors for this case have been compared to the filter's predicted standard deviations for these quantities. On average, the statistics of the along-track and altitude errors agree fairly well with the filter's modeled statistics, but the RMS cross-track error is almost three times larger than its predicted value. Although obviously suboptimal, this is a tolerable level of statistical mismatch, which is why the filter performs reasonably well.

The operation of the tracking sequencer for this case is illustrated by Fig. 3, which plots the PRN ID numbers of the tracked GPS satellites for the first 1.5 h of the filtering run. Each stair step on the plot corresponds to a tracking interval. There are approximately 48 stair steps per hour, consistent with the nominal schedule of 75 s/tracked satellite. Note that the PRN ID sequence follows a cyclical pattern: The numbers increase monotonically for subsequence lengths of between 2 and 6 tracking intervals until they approach the highest available PRN ID number, 31. Then the sequence drops down to a low PRN ID number to start a new cycle. Two important points to notice are the lack of data gaps and that most of the adjacent groups of four ID numbers correspond to four different GPS satellites. These two characteristics are important to achieving good observability of the system and, therefore, good accuracy. These characteristics are typical for LEO.

B. Convergence from Large Initial Position Errors

Some cases have been run to test the ability of the filter to converge from large initial position and velocity errors. In all of these cases, the truth orbit has an apogee altitude of 707 km, a perigee altitude of 366 km, and an inclination of 110 deg, but the filter's a priori state estimate starts at an altitude of 1000 km and with roughly the correct velocity to remain in a circular orbit at this higher altitude. In other respects these cases are similar to the example LEO case associated with Figs. 2 and 3.

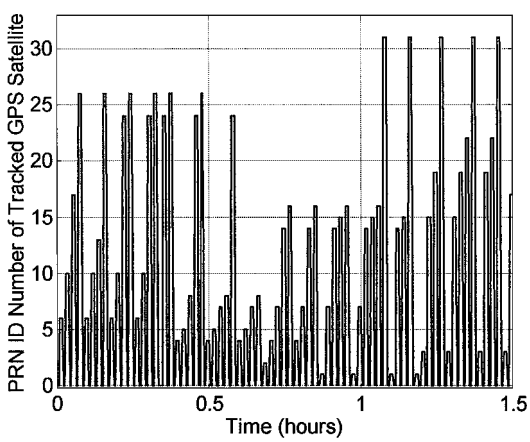

Fig. 3 Sequence of PRN ID numbers of tracked GPS satellites for typical LEO case.

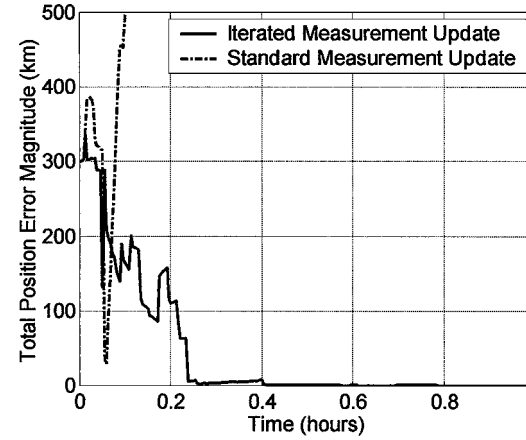

Fig. 4 Performance of two extended Kalman filters when starting from very large initial errors; one uses an iterated measurement update, and the other uses the standard update.

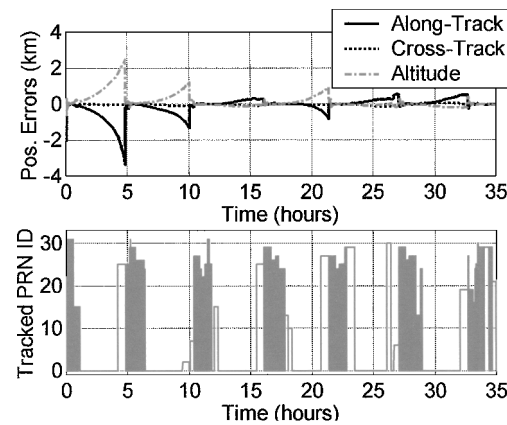

Fig. 5 Position error time histories (top plot) and associated sequence of tracked PRN ID numbers (bottom plot) for highly elliptical case whose apogee altitude is 18,107 km.

Figure 4 shows the initial performance of two different filters that operate on the same measurement data for one of these cases. The dash–dotted curve is for a filter that uses a standard measurement update, and the solid curve is for the iterated extended Kalman filter. The iterated filter converges in less than one-half of an hour, but the standard filter diverges after 6 min. of operation. Other cases have been tried with this same large initial estimation error. The iterated filter converges rapidly in every case, but the standard filter diverges in three out of four cases. Therefore, it is clear that the iterated filter is far superior in terms of convergence robustness. The ability to converge from a 300-km initial position error indicates that the iterated filter has a reasonable level of robustness and that it can be used safely in autonomous applications.

C. Performance as a Function of Orbit

A number of orbital inclinations, eccentricities, and altitudes have been investigated. The only orbital parameter that has a significant impact on system performance is altitude. The dominant altitude impact comes if the orbit extends above the altitude 3200 km, at which point there start to be long gaps when there are no GPS signals available because the user spacecraft passes outside of the primary gain pattern of the GPS satellites' broadcast antennas.

The filter has been tested on highly elliptical cases and on GEO cases to find out how it will perform when there are long data gaps. The performance degrades significantly in both of these situations. Figure 5 plots the position error component time histories for a highly elliptical case. Its perigee altitude is 1007 km, its apogee altitude is 18,107 km, and its inclination is 75 deg. The position error components are plotted on the top plot, and the sequence of tracked PRN ID numbers is plotted on the bottom plot. These results are for an iterated filter that uses both the carrier phase and pseudorange

measurements, and the receiver is assumed to use the TCXO oscillator. The filter's initial position and velocity errors for this case are 2 km and 0.7 m/s, respectively.

As is evident from Fig. 5, the performance for this case is significantly degraded. Notice that the vertical axis scale of the top plot is in kilometers rather than in meters. Even if one neglects the first orbit to allow for settling, the peak position errors are on the order of a kilometer, which is worse than the LEO performance by a factor of 10. It is evident from a comparison of the top and bottom plots that the large peak errors are caused by the long data gaps that occur near orbit apogee. The position errors on the top plot tend to diverge during the times when the bottom plot shows long gaps in the record of the tracked PRN ID numbers. During the low-altitude portions of the orbit, however, the accuracy of this case is comparable to that of the LEO cases.

The system performance is even further degraded in GEO. The best GEO results that have been achieved exhibit peak errors on the order of 7 km. The OXO had to be used for the receiver's oscillator to achieve even this poor level of performance; the filter has a tendency to diverge if the TCXO is used in GEO. The poorer GEO performance is the result of the very long data gaps that occur regularly at these high altitudes. The average time that is required to see four different GPS signals is on the order of 4 h. It is difficult to improve the GEO performance by going to a multichannel receiver because there are very few times when more than one GPS satellite signal is available with sufficient strength to be tracked by a conventional receiver.[22]

Note that the GEO case is the only one for which a large performance improvement has been realized through use of the OXO as the receiver clock. The LEO cases and the elliptical case show only moderate improvements from using the OXO.

A secondary altitude effect is present for LEO cases. For altitudes below 3200 km, there is a slight degradation in accuracy with a decrease in altitude. For example, a case with a perigee altitude of 985 km and an apogee altitude of 1007 km experienced a peak altitude error of 100 m. The peak altitude error increased to 144 m when the perigee and apogee altitudes decreased to 357 and 375 km, respectively. This modest performance degradation with decreases in altitude is probably the result of errors in the filter's orbital dynamics model. The model neglects Earth gravity terms above J_2, and the strength of these terms increases as altitude decreases.

D. Effect of Inaccuracy in the Filter's Orbital Dynamics Model

An improvement in the accuracy of the filter's dynamics model can significantly improve its performance. This has been demonstrated by tests in which the dynamic modeling mismatch between the truth model and the filter has been reduced to about 10^{-7} m/s^2. In GEO this reduces the peak steady-state position error from 7 km to about 400 m. The peak errors are reduced from about 100 to about 20 m in LEO. To achieve these improvements in the LEO cases, one would have to add a significant number of terms to the filter's spherical harmonic expansion of the Earth's gravitational field. In GEO one would have to include solar and lunar gravity models.

These approaches run counter to this system's philosophy of reducing computational load. If one needs more accuracy in LEO, then perhaps one should go to a multichannel receiver. In GEO, however, a conventional multichannel receiver will not be of much help, and one may be forced to make the requisite improvements in the dynamics model.

E. Usefulness of Carrier Phase Measurements

This study has considered whether the use of carrier phase measurements in the Kalman filter improves this system's performance. The answer is definitely not. The use of carrier phase data has not yielded consistent accuracy improvements in the cases that have been considered. In fact, the filter that does not use carrier phase sometimes performs better than the one that uses it.

F. Dependence of Performance on Miscellaneous Filter/Receiver Properties

There are additional system design parameters that affect accuracy. The use of longer tracking intervals for individual GPS signals leads to a degradation of accuracy in LEO cases. For example, if one uses 300 s per tracked signal as opposed to this study's nominal value of 75 s, then the LEO accuracy degrades by a factor of about two to yield peak per-axis errors on the order of 230 m and per-axis rms errors on the order of 60–70 m. This suggests that it would be a good idea to shorten the nominal tracking interval to something less than 75 s. Unfortunately, there is a limit to how much one can shorten this interval due to the need to allow adequate time for acquisition and due to the need to decode the 30-s navigation message.

There is some evidence that use of a shorter sample interval, 5 s as opposed to 15 s, may slightly improve performance. This change also triples the computational cost of the filter. The possibility of modest improvements is probably not worth the cost of switching to the shorter sampling period.

G. Computational Burden of Kalman Filter

In most cases considered, the Kalman filter requires an average computation rate of less than 3000 floating point operations per second (FLOPS). This value encompasses all propagation and measurement update operations, including numerical integration of the equations of motion. It corresponds to a 15-s measurement sample period with a single fourth/fifth-order Runge–Kutta numerical integration step per sample interval. If carrier phase measurements are not used, then the computational cost gets reduced by 5–10%. If the iterated nonlinear measurement update is used, then the computational cost increases by about 10% and may be slightly more than 3000 FLOPS. If the sample interval gets reduced, then the computational cost increases in inverse proportion to the interval's length. Note that the 3000-FLOPS value does not include the cost of the calculation of GPS satellite locations from the ephemeris data.

Use of this system will provide tremendous savings in terms of computational cost. The 3000-FLOPS value is probably less than the cost of running the 1000-Hz signal tracking loop for a single channel of a normal receiver. Thus, if one reduces from a 10-channel receiver to a single-channel receiver, then the savings in carrier tracking alone will be on the order of 80% or more even after one accounts for the added cost of running the Kalman filter. Furthermore, the reduction from 10 channels to 1 channel implies that most other computations, such as the calculation of GPS satellite locations, will be reduced by a factor of 10. Thus, the present system is expected to save more than 80% of the total computational load. This savings will allow the use of a much slower clock speed for the receiver's microprocessor, which will translate proportionally into reduced power consumption.

V. Summary

A new system has been proposed for performing autonomous orbit determination for Earth-orbiting spacecraft. It consists of a single-channel GPS receiver coupled to an extended Kalman filter. The receiver tracks a different GPS satellite once every 75 s and sends pseudorange measurements to the Kalman filter along with the location of the tracked GPS satellite. The Kalman filter processes these measurements sequentially to estimate the user spacecraft's position and velocity along with the receiver clock's offset and drift rate. The Kalman filter relies on dynamic models of the orbital motion and of the receiver clock drift to propagate its estimates between samples. The filter uses a simple gravity model in its orbit propagation, one that includes only the $1/r^2$ and J_2 terms. One version of the filter uses an iterated nonlinear measurement update to increase its domain of convergence.

The motivation for examining this system has been to try to develop a low-power solution to the autonomous orbit determination problem. A single-channel receiver can use a slower microprocessor clock speed, which reduces its power consumption proportionally.

This system has been evaluated using a simulation study. The results are as follows: In LEO the system can operate successfully using a low-power temperature-compensated crystal oscillator for its receiver clock. The iterated version of the filter can reliably converge from initial position errors as large as 300 km. Peak steady-state per-axis position errors ranging from 78 to 144 m can be achieved in LEO. At geosynchronous altitudes, the system works poorly even when it incorporates an ovenized crystal oscillator. Its peak per-axis

position error can be as large as 7 km in this case. This poor performance is caused by two factors: the limited availability of strong GPS signals at geosynchronous altitudes and the filter's neglect of solar and lunar gravity terms in its orbital dynamics model.

Acknowledgments

This work was supported in part by NASA through Grant NAG5-8788. Seymor Kant was the NASA Grant Monitor. Hee Jung, a graduate student at Cornell, helped to develop the code for the truth-model simulation's spherical harmonic expansion of the Earth's gravitational field.

References

[1]Hofmann-Wellenhof, B., Lichtenegger, H., and Collins, J., *GPS, Theory and Practice*, Springer-Verlag, New York, 1997, pp. 181–183.

[2]Wertz, J. R., and Larson, W. J. (eds.), *Space Mission Analysis and Design*, Kluwer, Boston, 1999, pp. 409–418.

[3]Akos, D. M., Normark, P.-L., Enge, P., Hansson, A., and Rosenlind, A., "Real-Time GPS Software Radio Receiver," *Proceedings of the ION National Technical Meeting*, Inst. of Navigation, Alexandria, VA, 2001, pp. 809–816.

[4]Wu., S. C., Yunck, T. P., and Thornton, C. L., "Reduced-Dynamic Technique for Precise Orbit Determination of Low Earth Satellites," *Journal of Guidance, Control, and Dynamics*, Vol. 14, No. 1, 1991, pp. 24–30.

[5]Yunck, T. P., Bertiger, W. I., Wu, S. C., Barsever, Y. E., Christensen, E. J., Haines, B. J., Lichten, S. M., Muellerschoen, R. J., Vigue, Y., and Willis, P., "1st Assessment of GPS-Based Reduced Dynamic Orbit Determination on TOPEX POSEIDON," *Geophysical Research Letters*, Vol. 21, No. 7, 1994, pp. 541–544.

[6]Chao, C. C., and Bernstein, H., "Onboard Stationkeeping of Geosynchronous Satellites Using a Global Positioning System Receiver," *Journal of Guidance, Control, and Dynamics*, Vol. 17, No. 4, 1994, pp. 778–786.

[7]Reichert, A., Axelrad, P., Wu, S. C., Bertiger, W., and Srinivasan, J., "Initial Demonstration of a Point Solution Algorithm for Orbit Determination Using the MicroGPS Receiver," *Proceedings of the ION National Technical Meeting*, Inst. of Navigation, Alexandria, VA, 1997, pp. 377–386.

[8]Moreau, M., Axelrad, P., Garrison, J. L., Kelbel, D., and Long, A., "GPS Receiver Architecture and Expected Performance for Autonomous GPS Navigation in Highly Eccentric Orbits," *Proceedings of the ION 55th Annual Meeting*, Inst. of Navigation, Alexandria, VA, 1999, pp. 653–665.

[9]Bierman, G. J., *Factorization Methods for Discrete Sequential Estimation*, Academic International Press, New York, 1977, pp. 69–76, 115–122.

[10]Psiaki, M. L., Theiler, J., Bloch, J., Ryan, S., Dill, R. W., and Warner, R. E., "ALEXIS Spacecraft Attitude Reconstruction with Thermal/Flexible Motions Due to Launch Damage," *Journal of Guidance, Control, and Dynamics*, Vol. 20, No. 5, 1997, pp. 1033–1041.

[11]Brown, R. G., and Hwang, P. Y. C., *Introduction to Random Signals and Applied Kalman Filtering*, 3rd ed., Wiley, New York, 1997, pp. 428–432.

[12]U.S. Standard Atmosphere, 1976, National Oceanic and Atmospheric Administration, 1976.

[13]Parkinson, B. W., "GPS Error Analysis," *Global Positioning System: Theory and Applications*, Vol. 1, edited by B. W. Parkinson and J. J. Spilker Jr., AIAA, Reston, VA, 1996, pp. 469–483.

[14]Yunck, T. P., "Orbit Determination," *Global Positioning System: Theory and Applications*, Vol. 2, edited by B. W. Parkinson and J. J. Spilker Jr., AIAA, Reston, VA, 1996, pp. 559–592.

[15]Kailath, T., *Linear Systems*, Prentice–Hall, Englewood Cliffs, NJ, 1980, pp. 615–618.

[16]Gill, P. E., Murray, W., and Wright, M. H., *Practical Optimization*, Academic International Press, New York, 1981, pp. 88–93, 134–136.

[17]Cohen, C. E., "Attitude Determination," *Global Positioning System: Theory and Applications*, Vol. 2, edited by B. W. Parkinson and J. J. Spilker Jr., AIAA, Reston, VA, 1996, pp. 519–538.

[18]"EGM96, The NASA GSFC and NIMA Joint Geopotential Model," NASA Goddard Space Flight Center, Greenbelt, MD; URL: http://cddisa.gsfc.nasa.gov/926/egm96/egm96.html, [cited 25 Nov. 2001].

[19]"GPS Almanacs," U.S. Coast Guard Navigation Center, URL: http://www.navcen.uscg.gov/gps/default.htm [cited 25 Nov. 2001].

[20]Zumberge, J. F., and Bertiger, W. I., "Ephemeris and Clock Navigation Message Accuracy," *Global Positioning System: Theory and Applications*, Vol. 1, edited by B. W. Parkinson and J. J. Spilker Jr., AIAA, Reston, VA, 1996, pp. 585–599.

[21]Klobuchar, J. A., "Ionospheric Effects on GPS," *Global Positioning System: Theory and Applications*, Vol. 1, edited by B. W. Parkinson and J. J. Spilker Jr., AIAA, Reston, VA, 1996, pp. 485–515.

[22]Long, A., Kelbel, D., Lee, T., Garrison, J., and Carpenter, J. R., "Autonomous Navigation Improvements for High-Earth Orbiters Using GPS," Centre National d'Etudes Spatiales Paper MS00/13, June 2000.